

Supporting Information

An X-ray Scattering and Quasielastic Neutron Scattering Study on the Structure and Dynamic Properties of Low- Temperature Methanol Confined in Ordered Microporous Carbon and Mesoporous Organosilica Pores

Hongyan Liu^a, Zhuanfang Jing^a, Keke Chai^{a,c}, Yongquan Zhou^{*a}, Koji Yoshida^b,
Takeshi Yamada^d, Toshio Yamaguchi^{*a,b}

^aKey Laboratory of Comprehensive and Highly Efficient Utilization of Salt Lake
Resources, Key Laboratory of Salt Lake Resources Chemistry of Qinghai Province,
Qinghai Institute of Salt Lakes, Chinese Academy of Sciences, Xining, Qinghai,
810008, China

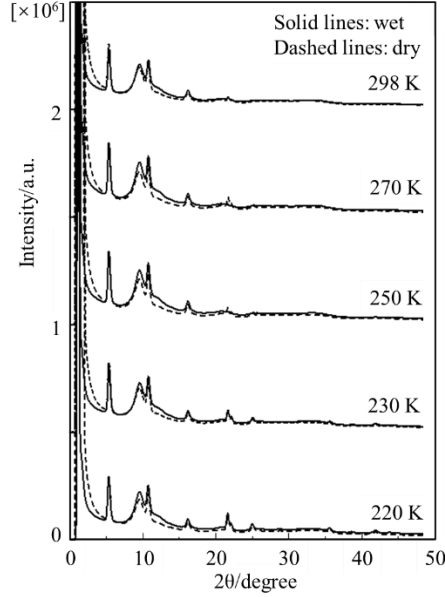
^bDepartment of Chemistry, Faculty of Science, Fukuoka University, Nanakuma,
Jonan, Fukuoka, 814-0180, Japan

^cUniversity of Chinese Academy of Sciences, Beijing 100049, China

^dNeutron Science and Technology Center, Comprehensive Research Organization for
Science and Society, 162-1 Shirakata, Tokai 319-1106, Japan

*All correspondence should be sent to: Prof. Toshio Yamaguchi and Prof. Yongquan
Zhou. E-mail: yamaguch@fukuoka-u.ac.jp and yongqzhou@163.com.

1 **Part 1 Experimental scattered intensities of wet and dry Ph-PMO samples at**
2 **different temperatures**



3
4 **Fig.S1** Experimental scattered intensities of wet (solid lines) and dry (dashed lines) Ph-PMO
5 samples at different temperatures.

6 **Part 2 Large-angle X-ray scattering data analysis**

7 The X-ray scattering intensities of methanol-absorbed (wet) in Ph-PMO, $I_s(s)$,
8 can be described by Eq. S1,

$$9 \quad I_s(s) = I_{\text{MeOH}}(s) + I_{\text{MeOH-PMO}}(s) + I_{\text{PMO}}(s) + I_c(s) \quad (\text{S1})$$

10 where $I_{\text{MeOH}}(s)$ and $I_{\text{PMO}}(s)$ represent X-ray scattering intensities from adsorbed
11 methanol and Ph-PMO, respectively. $I_{\text{MeOH-MCM}}(s)$ denotes the intensities from
12 interactions between adsorbed methanol and the Ph-PMO surface, and $I_c(s)$ represents
13 those from the capillary.

14 The X-ray intensities of the dry Ph-PMO sample, $I_{\text{dry}}(s)$, can be represented as

$$15 \quad I_{\text{dry}}(s) = I_{\text{PMO}}(s) + I_c(s) \quad (\text{S2})$$

16 Therefore, the X-ray scattering intensities related to the adsorbed methanol in

1 Ph-PMO pores are obtained by subtracting Eq. S2 from Eq. S1 as

$$2 \quad I_s(s) - I_{\text{dry}}(s) = I_{\text{MeOH}}(s) + I_{\text{MeOH-PMO}}(s) \quad (\text{S3})$$

3 As previously described, the experimental X-ray intensities, $I_s(s)$, were corrected
4 for multiple and Compton scattering.^{1,2} The structure function, $i(s)$, is given by Eq.
5 S4.

$$6 \quad i(s) = KI_s(s) - \sum x_i f_i^2(s) = K[I_{\text{MeOH}}(s) + I_{\text{MeOH-PMO}}(s)] - \sum x_i f_i^2(s) \quad (\text{S4})$$

7 Here, K represents a factor to normalize the experimental intensities to absolute units
8 in a usual manner.^{1,2} x_i is the number of atoms i in a stoichiometric volume, V ,
9 containing one O atom from a methanol molecule. $f_i(s)$ represents the atomic
10 scattering factor of atom i corrected for the anomalous dispersion.

11 The radial distribution function (RDF), $D(r)$, was calculated by means of the
12 Fourier transform as

$$13 \quad D(r) = 4\pi r^2 \rho_0 + 2r\pi^{-1} \int_0^{s_{\text{max}}} si(s)M(s)\sin(rs)ds \quad (\text{S5})$$

14 Here, $\rho_0 (= [\sum x_i f_i^2(0)]/V)$ stands for the average scattering density of a sample in
15 the stoichiometric volume V , and s_{max} is the maximum s value used in the analysis
16 ($s_{\text{max}} = 14.4 \text{ \AA}^{-1}$). $M(s)$ is a modification function expressed as

$$17 \quad M(s) = [\sum x_i f_i^2(0) / \sum x_i f_i^2(s)] \exp(-0.01s^2) \quad (\text{S6})$$

18 All treatments of the X-ray diffraction data were carried out with the KURVLR
19 program.²

20 **Part 3 Dynamic susceptibilities of methanol confined in OMC and Ph-PMO**
21 **pores at 300, 285, and 270 K**

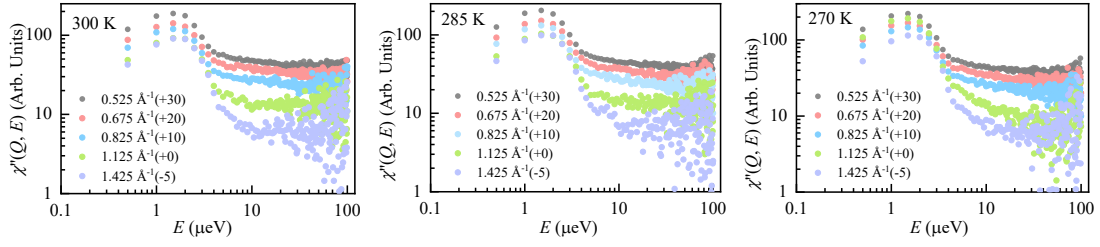


Fig. S2 Dynamic susceptibilities for methanol confined in OMC pores at different Q 's at 300, 285, and 270 K, and add a different value to the $\chi''(Q, E)$.

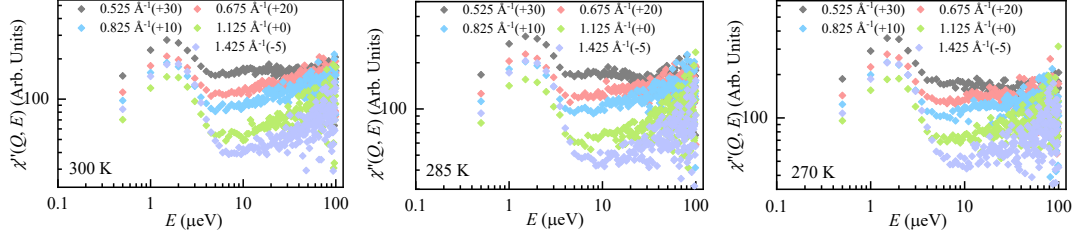


Fig. S3 Dynamic susceptibilities for methanol confined in Ph-PMO pores at different Q 's at 300, 285, and 270 K, and add a different value to the $\chi''(Q, E)$.

Part 4 Fitting results of QENS spectra measurement at 300, 285, and 270 K.

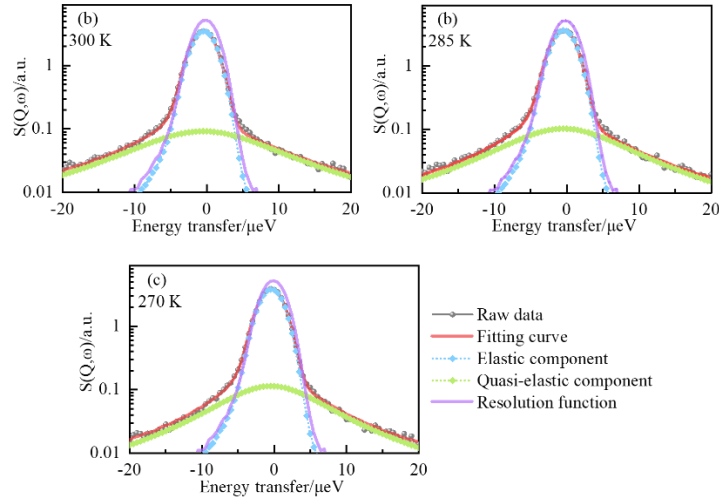


Fig. S4 Fitting results of the QENS spectra of methanol confined in OMC pores at $Q=0.825 \text{ \AA}^{-1}$ and at 300 K (a), 285 K (b), and 270 K (c). The gray line is the experimental values, the red line is the fitted data, the green dotted line is a quasielastic component, the blue dotted line is the elastic component, and the purple line is the resolution function.

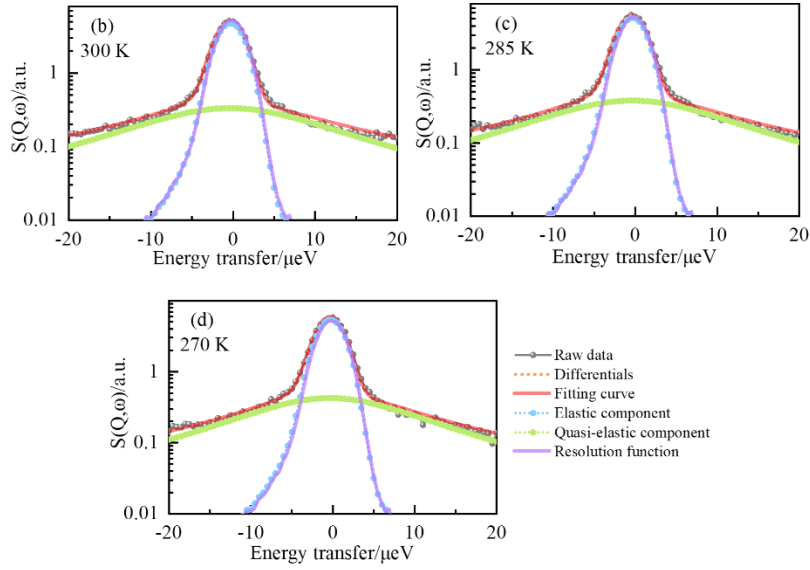


Fig. S5 Fitting results of the QENS spectra of methanol confined in PMO pores at $Q=0.825 \text{ \AA}^{-1}$ and at 300 K (a), 285 K (b), and 270 K (c). The gray line is the experimental values, the red line is the fitted data, the green dotted line is a quasielastic component, the blue dotted line is the elastic component, and the purple line is the resolution function.

Part 5 Nonlinear fitting of the $\Gamma(Q)$ function at each temperature for methanol confined in OMC and Ph-PMO pores.

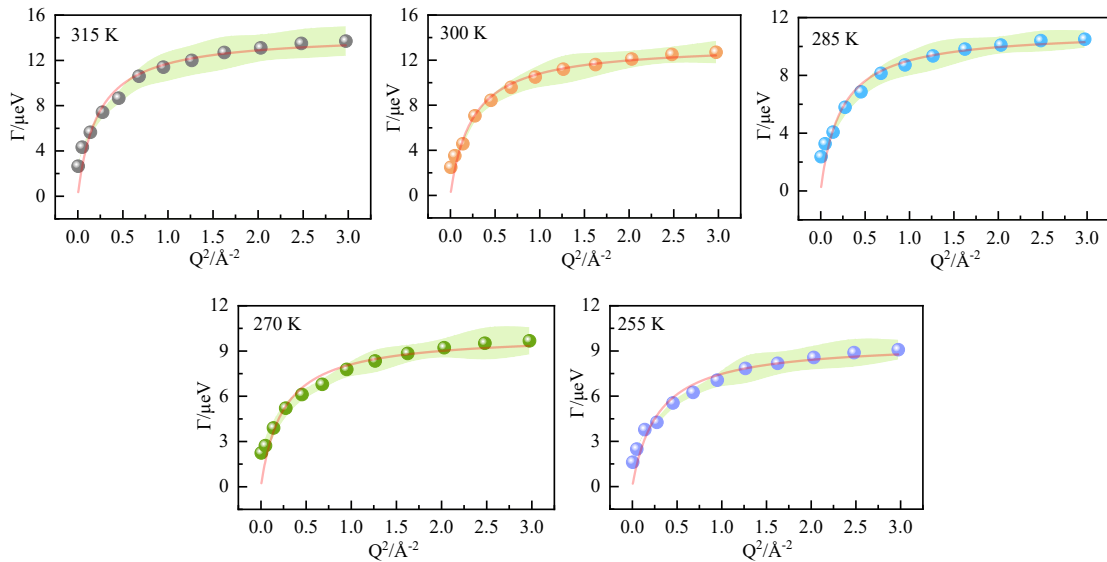


Fig. S6 The half-width at half-maximum (ball) of the QENS spectra for methanol confined in OMC pores at 315, 300, 285, 270, and 255 K. The red lines indicate a nonlinear fitting. Light green shading indicates error.

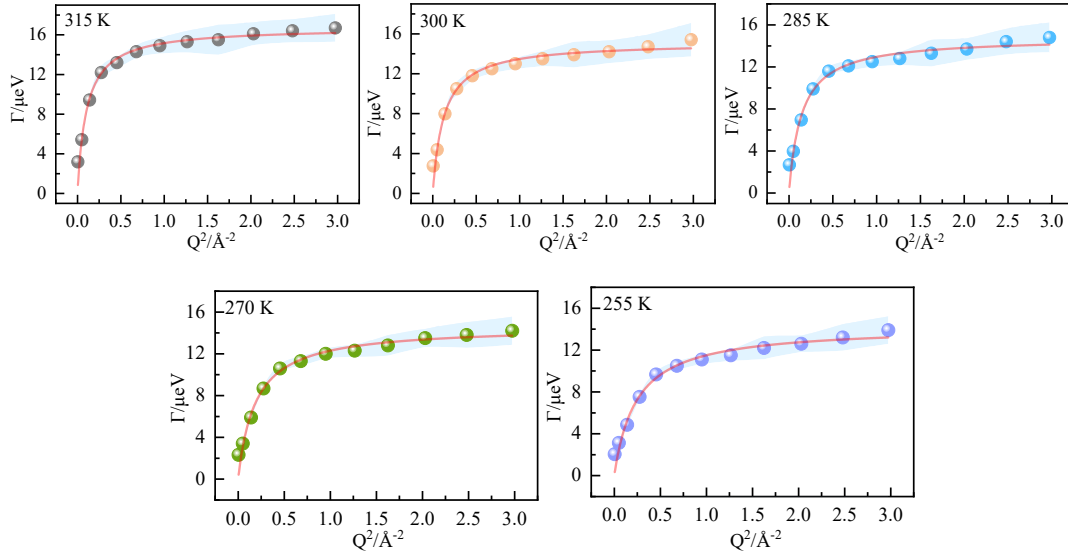


Fig. S7 The half-width at half-maximum (ball) of the QENS spectra for methanol molecules confined in Ph-PMO pores at 315, 300, 285, 270, and 255 K. The red lines indicate a nonlinear fitting. Light blue shading indicates error.

Part 6: The measured diffusion coefficients of methanol molecules in OMC and Ph-PMO pores.

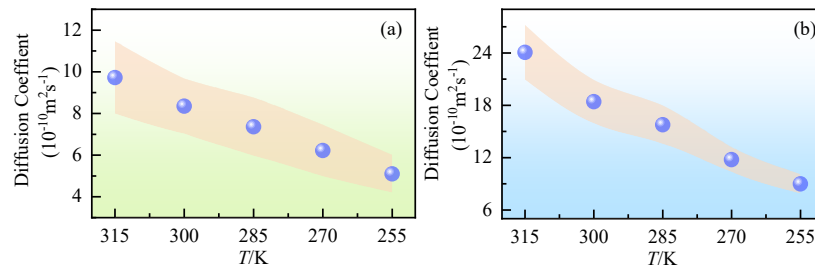


Fig. S8 The diffusion coefficient as a function of temperature for methanol confined in OMC (a) and Ph-PMO (b). Light orange shading indicates error.

Part 7: Elastic Incoherent Structure Factor (EISF) Fitting.

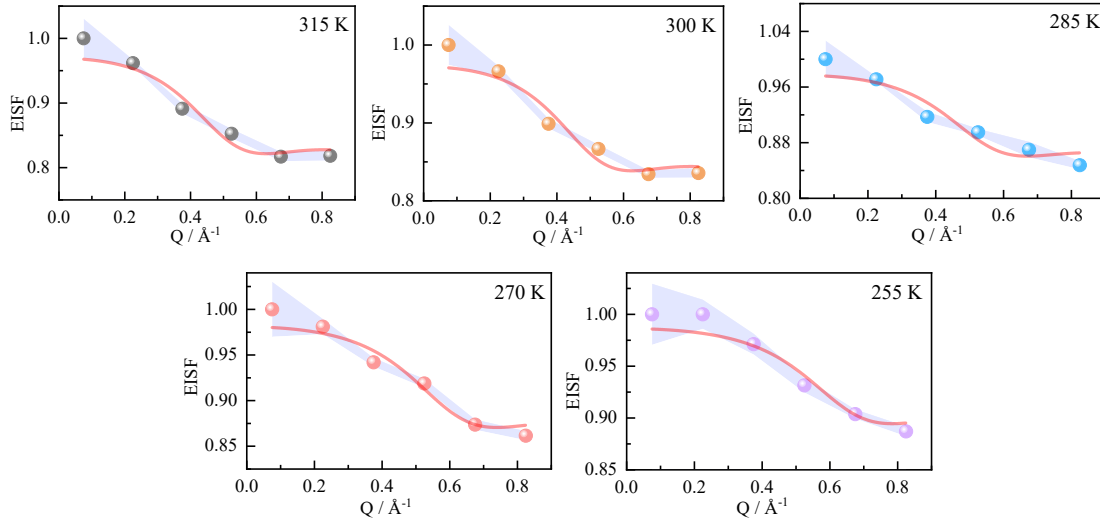


Fig. S9 Elastic incoherent structure factor (EISF) for methanol at various temperatures measured in OMC pores with $Q < 0.9 \text{ \AA}^{-1}$. The red solid lines represent fits to the EISF model, the light purple shading indicates error.

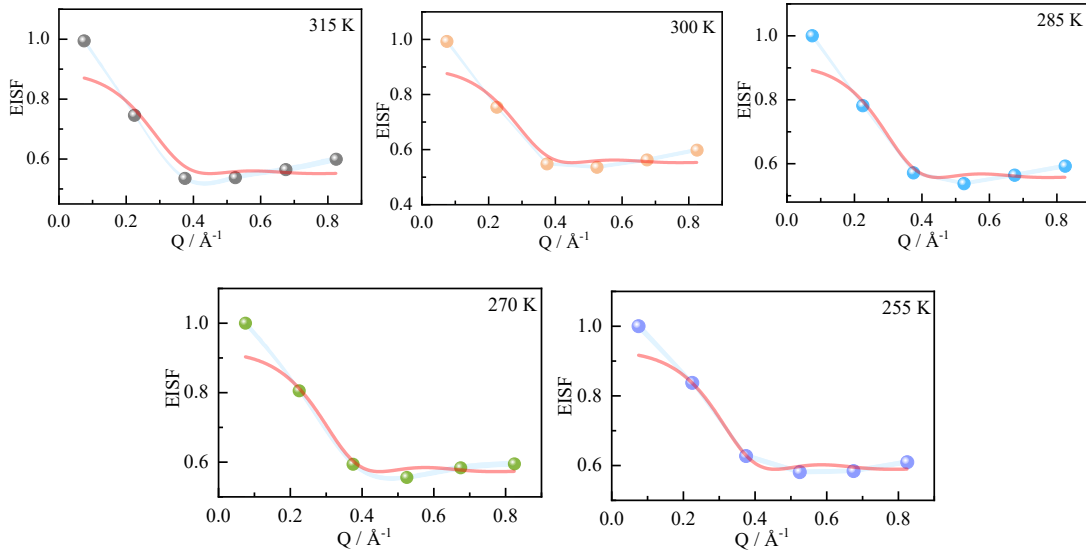


Fig. S10 Elastic incoherent structure factor (EISF) for methanol at various temperatures measured in Ph-PMO pores with $Q < 0.9 \text{ \AA}^{-1}$. The red solid lines represent fits to the EISF model. The light blue shading indicates an error.

To further comprehend the concept of dynamic states distinguished by the mobility of water molecules, we calculated the elastic incoherent structure factor (EISF), which is derived from the elastic and quasielastic components of the

1 experimental data. It is defined as the fraction of elastic intensity in the QENS spectra.

2 ³ In Fig. S10 and Fig. S10, we show the EISFs derived from the QENS measurements
 3 as a function of Q at different temperatures. The decrease in the EISF with an increase
 4 in temperature suggests that the fraction of immobile H atoms decreases. As shown in
 5 Figs. 6(a) and 6(d) found that the behavior of HWHM is characteristic of diffusion of
 6 water protons confined in a volume assimilated to a sphere of confinement radius a ,
 7 which was confirmed by the fitting of EISF. For such a situation, the EISF can be
 8 given by

$$9 \quad EISF = p_0 + (1 - p_0) \left[\frac{3j_1(Qa)}{Qa} \right]^2 = p_0 + (1 - p_0) \left[\frac{3}{Qa} \left(\frac{\sin(Qa)}{(Qa)^2} - \frac{\cos(Qa)}{(Qa)} \right) \right]^2 \quad (S9)$$

10 where j_1 stands for the first-order spherical Bessel function, and p_0 is the fraction of
 11 “immobile” hydrogens that do not participate in the confined diffusion.^{4,5} We found
 12 that we obtained rather poor fits when fitting the EISF to this equation. Especially
 13 when Q is close to 0, the EISF does not approach unity as expected from Eq. (S9).
 14 This is because the immobilized/confined water molecules constitute only a fraction c
 15 of the system. In contrast, a fraction $1-c$ participates in jump diffusion, as seen from
 16 HWHM fits or in free diffusion.

17 In this condition, writing Eq.(2) separately for the two species, and taking $I'(Q, E)$
 18 $= C(Q)\delta(E) + (1-C(Q))S(Q, E)$, we can write⁶

$$19 \quad I'_b(Q, E) = A_b(Q)\delta(E) + (1 - A_b(Q))S_b(Q, E) \quad (S10)$$

$$20 \quad I'_f(Q, E) = A_f(Q)\delta(E) + (1 - A_f(Q))S_f(Q, E) \quad (S11)$$

$$21 \quad I'(Q, E) = cI'_b(Q, E) + (1 - c)I'_f(Q, E) \quad (S12)$$

22 Here, the subscripts “b” and “f” denote bound (including immobilized and confined

1 water molecules) and free (including jump diffusion and free diffusion water
2 molecules), respectively. For free water molecules, assuming that the EISF $A_f = 0$ is
3 reasonable. Additionally, we anticipate that $\int S(Q,E)dE = \text{const} = 1-c$, indicating that the
4 area of $S(Q,E)$ remains constant regardless of Q and solely depends on the mobile
5 fraction. For the confined water, the motion of the locally confined water molecules is
6 likely rapid, resulting in a broad Lorentzian that may not be measurable within the
7 energy resolution of the instrument. Consequently, we can take $S_b(Q,E) \approx 0$, as the
8 corresponding signal is most likely absorbed into the background $B(Q,E)$. Based on
9 this, we can write for the EISF

$$10 \quad \text{EISF}' = \frac{A(Q)}{\int (A(Q)\delta(E) + S(Q,E))dE} = \frac{cA_b(Q)}{cA_b(Q) + (1-c)} \quad (\text{S13})$$

11 Substitute the expression for EISF in Eq. (S9) for $A_b(Q)$ in Eq. (13), and obtained the
12 fits results.

13 **Part 8. References**

- 14 1. K. Furukawa, *Rep. Prog. Phys.*, 1962, **25**, 395.
- 15 2. G. Johansson, *Chem. Scr.*, 1973, **4**, 195.
- 16 3. U. R. Shrestha, D. Bhowmik, J. R. Copley, M. Tyagi, J. B. Leão, X. Q. Chu, *Pro.*
17 *Nat. Acad. Sci.*, 2015, **112**, 13886-13891.
- 18 4. K. Ito, K. Yoshida, M. C. Bellissent-Funel, T. Yamaguchi, *Bulletin of the Chem.*
19 *Soc. Japan*, 2014, **87**, 603-608.
- 20 5. J. Jacobsen, M. S. Rodrigues, M. T. Telling, A. L. Beraldo, S. F. Santos, L. P.
21 Aldridge, H. N. Bordallo, *Sci. Rep.*, 2013, **3**, 2667.
- 22 6. G. R. Acharya, M. Tyagi, E. Mamontov, P. M. Hoffmann, *J. Phys. Chem. B*, 2023,
23 **127**, 7384-7393.